Model-based analysis of clinical fluorescence spectroscopy for *in vivo* detection of cervical intraepithelial dysplasia

Sung K. Chang
Massachusetts General Hospital
Wellman Center for Photomedicine
Boston, Massachusetts 02114

Nena Marin
The University of Texas at Austin
Department of Biomedical Engineering
Austin, Texas 78712

Michele Follen
The University of Texas M.D. Anderson Cancer Center
Department of Gynecologic Oncology
Houston, Texas 77030

Rebecca Richards-Kortum
Rice University
Department of Bioengineering
Houston, Texas 77251
E-mail: rkortum@rice.edu

Abstract. We present a mathematical model to calculate the relative concentration of light scatterers, light absorbers, and fluorophores in the epithelium and stroma. This mathematical description is iteratively fit to the fluorescence spectra measured *in vivo*, yielding relative concentrations of each molecule. The mathematical model is applied to a total of 493 fluorescence measurements of normal and dysplastic cervical tissue acquired *in vivo* from 292 patients. The estimated parameters are compared with histopathologic diagnosis to evaluate their diagnostic potential. The mathematical model is validated using fluorescence spectra simulated with known sets of optical parameters. Subsequent application of the mathematical model to *in vivo* fluorescence measurements from cervical tissue yields fits that accurately describe measured data. The optical parameters estimated from 493 fluorescence measurements show an increase in epithelial flavin adenine dinucleotide (FAD) fluorescence, a decrease in epithelial keratin fluorescence, an increase in epithelial light scattering, a decrease in stromal collagen fluorescence, and an increase in stromal hemoglobin light absorption in dysplastic tissue compared to normal tissue. These changes likely reflect an increase in the metabolic activity and loss of differentiation of epithelial dysplastic cells, and stromal angiogenesis associated with dysplasia. The model presented here provides a tool to analyze clinical fluorescence spectra yielding quantitative information about molecular changes related to dysplastic transformation. © *2006 Society of Photo-Optical Instrumentation Engineers.*
[DOI: 10.1117/1.2187979]

Keywords: fluorescence spectroscopy; diagnosis; cervical cancer.

Paper 05204RR received Jul. 26, 2005; revised manuscript received Nov. 11, 2005; accepted for publication Nov. 14, 2005; published online Mar. 27, 2006.

1 Introduction

Despite tremendous efforts to prevent and treat cancer, it remains the second leading cause of death in the United States. Screening for preinvasive cancer can improve the long-term outcome regarding morbidity and mortality if it is followed with appropriate therapy. However, the sensitivity and specificity of many screening tools for dysplasia are limited,[1] and as a result, opportunities for early detection are missed. Furthermore, due to the high cost of many screening tools, they are not available to all persons at risk. Optical spectroscopy represents a new screening tool for early dysplasia that has the potential to address these limitations. Optical spectroscopy of tissue provides quantitative information that can be analyzed, instantaneously producing an objective diagnosis even in the hands of a nonexpert operator. Devices to make these measurements have become inexpensive, robust, and portable because of advances in computing, fiber optics, and semiconductor technology.

Optical spectroscopy uses the interaction of light and tissue to make an immediate diagnosis.[2] A fiber optic probe emitting low-power light is placed on the tissue, and the spectrum of remitted light is rapidly measured.[3] Optical spectroscopy is sensitive to changes that are intimately related to the dysplasia-to-carcinoma sequence, including epithelial cell metabolism, angiogenesis, nuclear size, and texture. In particular, fluorescence spectroscopy has shown promise as an effective diagnostic tool for dysplasia in a variety of organ sites, including the cervix,[4–7] breast tissue,[8] and the oral cavity,[9,10] where the diagnostic sensitivity and specificity ranges between 70 and 90%, in some cases reaching more than 95%.

The diagnostic capability of fluorescence spectroscopy originates from the optical contrast between normal and dysplastic tissue at the molecular level. Important sources of intrinsic fluorescence in the epithelium include the mitochondrial cofactors, reduced nicotinamide adenine dinucleotide (NADH) and flavin adenine dinucleotide (FAD). Normal and cancerous cell lines show statistically significant differences in cytoplasmic fluorescence due to the mitochondrial

fluorophores.[11,12] Differences in epithelial fluorescence have also been observed in fresh sections from normal and abnormal tissue;[13] cytoplasmic fluorescence that is limited to the basal layer in the normal epithelium is observed in the basal 1/3 to 2/3 of the epithelial thickness in mild and moderate dysplasia and throughout the whole epithelium in severe dysplasia and carcinoma *in situ*, suggesting an increase in metabolically active cells and loss of differentiation. At the same time, stromal fluorescence that originates from the collagen cross-links decreases in abnormal tissue compared to normal tissue,[13] possibly due to the breakdown of the extracellular matrix by preinvasive epithelial cells. The relative concentrations of NADH and collagen estimated from *in vivo* fluorescence measurements can serve as important diagnostic markers. In one study, a diagnostic algorithm based on these two parameters yielded a sensitivity and specificity of 62 and 92%, respectively, in discriminating cervical SILs (squamous intraepithelial lesions) from squamous normal and metaplastic tissue.[14]

Other physiologic processes can alter the concentration of these fluorophores. For example, increasing age and menopause are associated with an increase in stromal fluorescence as well as a corresponding decrease in epithelial fluorescence.[15] In addition, small changes in epithelial fluorescence of cervical tissue are observed throughout the menstrual cycle.[16] These variations cause interpatient and intrapatient variability that can complicate the development of robust diagnostic algorithms based on fluorescence measurements from tissue.

Tissue fluorescence spectra are also affected by optical events such as absorption and scattering, and these optical properties have been shown to change with dysplastic progression. Theoretical and experimental studies of normal and dysplastic cells have shown that nuclear atypia associated with dysplastic progression increases light scattering due to cellular nuclei.[17–20] A significant light absorber in tissue is hemoglobin in the stromal vasculature; increased light absorption in abnormal tissue due to angiogenic developments has been quantified using diffuse reflectance measurements.[21]

Fluorescence spectroscopy can probe the optical characteristics of tissue that are correlated with dysplastic progression; thus, fluorescence spectroscopy has the potential to monitor changes in these biomarkers for diagnostic purposes. A number of mathematical models have been developed to analyze fluorescence spectra of tissue to quantitatively extract information about optically active biomarkers of dysplasia. Most of these models estimate optical properties of bulk tissue by considering tissue as a one-layered medium.[14,22–24] However the optical properties in the epithelial and stromal layers are affected in opposing manners by different physiological changes; for example, epithelial fluorescence increases and stromal fluorescence decreases with dysplasia, but epithelial fluorescence decreases and stromal fluorescence increases with menopause. Thus, it is important to estimate the optical properties of the epithelium and the stroma separately, and models that assume tissue homogeneity may fail to correctly extract changes in these parameters, potentially limiting their diagnostic performance. More recently, Stasic et al.[25] developed a model to estimate the exogenous fluorophore concentrations in a two-layered medium from spatially resolved fluorescence measurements based on diffusion theory. Although

diffusion theory provides a good description of light propagation in turbid media and is applicable to the stroma, it does not accurately describe light propagation in the epithelium because of the low level of light scattering in this thin layer of tissue.

In this paper, we present a mathematical approach to estimate the relative fluorophore concentration, scattering, and absorption properties from fluorescence spectra of epithelial tissue. For clinical purposes, it is important to estimate the optical properties from fluorescence spectra of tissue that potentially yield diagnostically significant information. The mathematical approach described in this paper applies an analytical model of fluorescence[26] to estimate tissue optical parameters from clinically acquired fluorescence spectra of tissue. An important advantage of this approach is that optical properties of the epithelium and the stroma are estimated separately by differentiating the two layers in the model. After validation, the approach is applied to a large set of fluorescence measurements acquired *in vivo* from normal and dysplastic cervical tissue to quantitatively extract epithelial and stromal optical properties. These parameters are examined to determine whether they have diagnostic potential and to study the influence of age and menopausal status on these optical parameters. We find that changes in epithelial fluorescence and light scattering, stromal fluorescence, and hemoglobin light absorption in normal and dysplastic tissue correlate well with the increase in dysplastic cells in the epithelium and angiogenic developments in the stroma following dysplasia.

2 Materials and Methods

2.1 Study Protocol

The study protocol was reviewed and approved by the Institutional Review Boards at the University of Texas M.D. Anderson Cancer Center, the British Columbia Cancer Agency, Vancouver, Canada and the University of Texas at Austin. Eligible patients included those over the age of 18 who were not pregnant, and who were referred to the colposcopy clinic at the British Columbia Cancer Agency with an abnormal Papanicolaou smear. After signing informed consent, all patients underwent a demographic interview, risk factor questionnaire, complete history, and physical exam and pan-colposcopy of the vulva, vagina, and cervix. Initially, each patient underwent a urine pregnancy test and a Papanicolaou smear. The last menstrual period and menstrual history were asked of each patient.

During colposcopy, two colposcopically normal sites and one colposcopically abnormal site were chosen by the physician or nurse colposcopist, and fluorescence measurements were acquired from these three sites. It was noted whether these sites corresponded to squamous or columnar epithelium or the transformation zone. Following fluorescence measurement, each site was biopsied and submitted for histopathologic diagnosis. Each biopsy was read by the pathologist assigned to the case that day, and was subsequently reviewed by the study histopathologist. Discrepant cases were reviewed a third time for consensus diagnosis by the study histopathologist. Standard diagnostic criteria were used[27] and consensus diagnostic categories included: normal squamous epithelium, normal columnar epithelium, inflammation, metaplasia, squamous atypia, human papillomavirus (HPV)-associated

changes, grade 1 cervical intraepithelial neoplasia (CIN 1), grade 2 cervical intraepithelial neoplasia (CIN 2), and grade 3 cervical intraepithelial neoplasia (CIN 3). In subsequent analysis, normal squamous epithelium, inflammation, and metaplasia were grouped together as squamous normal (SN) tissue, squamous atypia, HPV-associated changes, and CIN 1 were grouped together as LGSIL (low-grade squamous intraepithelial lesion), and CIN 2 and CIN 3 were grouped together as HGSIL (high-grade squamous intraepithelial lesion).

2.2 Instrumentation

The device used to measure clinical fluorescence spectra consists of three components: (1) an arc lamp and filter wheel to provide excitation light, (2) a fiber optic probe to deliver the excitation light and collect fluorescent light from the measurement site, and (3) a spectrograph coupled to a CCD camera to acquire fluorescence spectra. Broad spectrum light from the 75-W xenon lamp (A-1010B and LPS220, Photon Technology Inc., Birmingham, New Jersey) is filtered through 24 bandpass filters (10 nm FWHM) to generate quasi-monochromatic excitation light between 300 and 530 nm at 10-nm intervals. The fiber optic probe consists of 25 excitation fibers and 12 collection fibers, arranged randomly on a 1.8-mm-diam quartz fiber at the tip. All optical fibers in the probe have a 200-μm-diam quartz core and a 0.2 numerical aperture (NA). The collected fluorescent light is guided to an imaging spectrograph (TRIAX 320, Jobin Yvon, Edison, New Jersey), and the resulting light spectrum is recorded using a thermoelectrically cooled CCD camera (DV-420, Andor Technology Ltd., S. Windsor, Connecticut). For quality control purposes, spectra are measured from calibration lamps, a set of positive, fluorescent standards as well as negative, nonfluorescent standards every 2 h (Ref. 28). A National Institute of Standards and Technology (NIST) traceable tungsten source (LS-1-CAL, Ocean Optics, Dunedin, Florida) is used to calibrate the spectral response of the system and a mercury argon lamp (HG-1, Ocean Optics, Dunedin, Florida) is used to perform wavelength calibration. The positive standard set includes Exalite 400, coumarin 480, and rhodamine 610 contained in 1-cm-path-length quartz cuvettes. Negative standards, where no fluorescence signal is expected, include deionized ultrafiltered water in a brown glass bottle and the surface of an empty frosted quartz cuvette.

Extensive calibration routines were performed on all data measured with the clinical device to ensure the quality of the absolute signal intensity and the spectral shape of the fluorescence spectra.[28] Briefly, the measured data were processed by (1) subtracting the background signal measured with the negative standard, (2) compensating for the variability in CCD camera sensitivity and lamp power output by normalizing with fluorescence intensity from a positive standard (rhodamine 610), and (3) calibrating the wavelengths using the peaks of the measured mercury argon lamp. To ensure the reproducibility of the calibration routine, daily measurements of the two positive standards (Exalite 400 and coumarin 480) were processed with the calibration routine and checked for abnormalities in signal intensity and spectral shape.

2.3 Mathematical Model for Parameter Estimation

A mathematical model was used to analyze fluorescence spectra acquired clinically to extract optical parameters associated with the epithelium and the stroma. In this analysis, an expression that describes the tissue fluorescence as a function of the optical properties of each layer was fit to the tissue spectra. Values of the optical properties were adjusted iteratively until the best agreement between predicted spectra and measured spectra was obtained in the least-squares sense. As a result of the fitting process, the set of tissue optical properties that give best agreement between a predetermined analytical expression, known as the forward model, and the measured spectra can be estimated.

Our group previously developed and validated an analytical, forward model to describe fluorescence spectra of two-layer media.[26] Briefly, the model describes the propagation of light in the epithelial layer with thickness D using exponential attenuation, while diffusion theory is used to describe light propagation in the underlying semiinfinite stromal layer. Optical properties within each layer are assumed to be homogeneous. In the model, the total detected fluorescence $F_{\text{total}}^{\text{detected}}$, is expressed as a sum of the fluorescence contributions from the epithelial and stromal layers:

$$F_{\text{total}}^{\text{detected}} = F_1^{\text{detected}} + F_2^{\text{detected}} + F_3^{\text{detected}} + F_4^{\text{detected}}. \quad (1)$$

Epithelial fluorescence is emitted isotropically as the excitation light I_0 incident on the tissue surface travels through the epithelium. Here, F_1^{detected} accounts for epithelial fluorescence that is remitted from the tissue surface:

$$F_1^{\text{detected}}(\lambda_x, \lambda_m) = \frac{1}{2} R_{\text{NA}} \int_0^D I_0 \exp(-\mu_{\text{eff1}}(\lambda_x)z)$$
$$\times \sum_{k=1}^N [\mu_{af1(k)}(\lambda_x)\phi_{f1(k)}(\lambda_x, \lambda_m)]$$
$$\times \exp[-\mu_{\text{eff1}}(\lambda_m)z]\mathrm{d}z, \quad (2)$$

where μ_{s1}, μ_{a1}, μ_{af1}, and ϕ_{f1} are scattering coefficient, total absorption coefficient, absorption coefficient of the fluorophore, and quantum efficiency of the fluorophore, respectively, in the epithelium; and R_{NA} accounts for the solid angle subtended by the NA of the detection fiber. Half of the isotropically emitted epithelial fluorescence is initially directed downward to the stroma, a portion of this fluorescence is subsequently backscattered into the epithelium, $F'^-_{\text{epi}}(z=D)$. The detected portion of this fluorescence is given by

$$F_2^{\text{detected}}(\lambda_x, \lambda_m) = R_{\text{NA}}\{F'^-_{\text{epi}}(z=D)\exp[-\mu_{\text{eff1}}(\lambda_m)D]\}. \quad (3)$$

Similarly, a portion of the incident excitation light travels through the epithelial layer, and is backscattered by the stromal layer I'_s. Epithelial fluorescence collected as a result of the backscattered excitation light is given by:
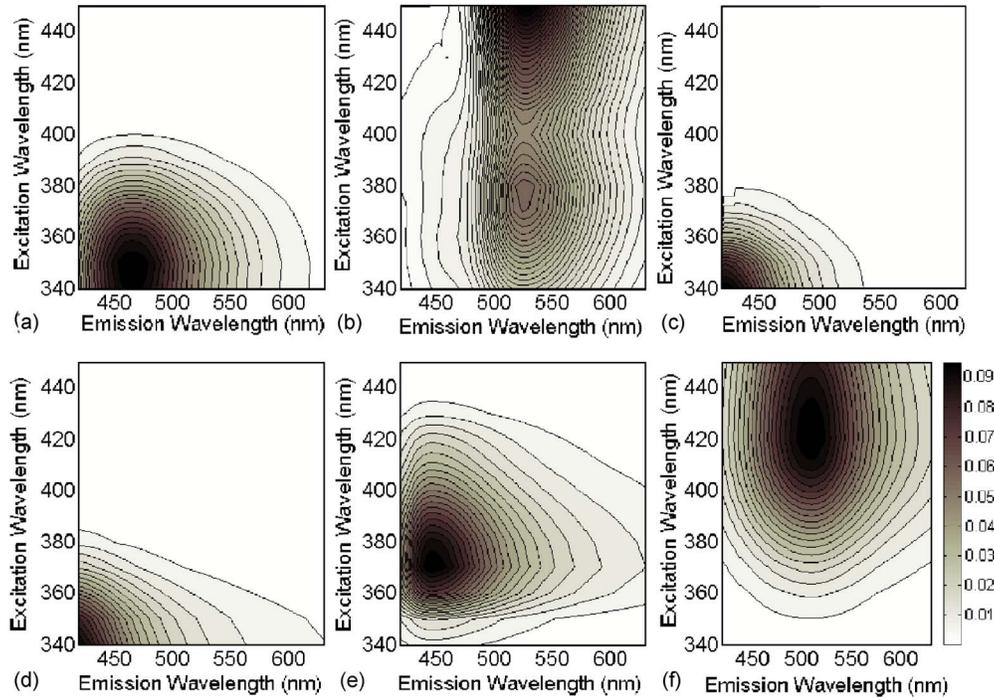
Fig. 1 Fluorescence EEMs of the fluorophores included in the mathematical model. Top row shows epithelial fluorophores (a) NADH, (b) FAD, and (c) keratin. Bottom row shows (d) component 1, (e) component 2, and (f) component 3 of stromal fluorescence. All EEMs were normalized to maximum intensity. Contour lines connect points of equal fluorescence intensity and scale bar on the lower right shows relative fluorescence intensity.

$$F_3^{\text{detected}}(\lambda_x, \lambda_m) = R_{\text{NA}} \int_0^D I_s'^{-}(z = D)$$

$$\times \exp(-\mu_{\text{eff1}}(\lambda_x)z)$$

$$\times \sum_{k=1}^{N} [\mu_{af1(k)}(\lambda_x) \phi_{f1(k)}(\lambda_x, \lambda_m)]$$

$$\times \exp[-\mu_{\text{eff1}}(\lambda_m)(D-z)]dz. \qquad (4)$$

Stromal fluorescence F_4^{detected} is described as

$$F_4^{\text{detected}}(\lambda_x, \lambda_m) = [R_{\text{NA}} \bar{F}_{\text{str}}(\lambda_x, \lambda_m)]\exp[-\mu_{\text{eff1}}(\lambda_m)D],$$

$$(5)$$

where $\bar{F}_{\text{str}}$ is the stromal fluorescence remitted at the stromal surface. Within each layer, it is necessary to specify fluorophores, absorbers, and scatterers included, as well as their wavelength-dependent optical properties. However, the magnitude of each parameter is allowed to vary to give the best agreement between the analytic expression and the measured data.

Within the epithelium, the model includes contributions from the fluorophores NADH, FAD, and keratin. Fluorescence characteristics of NADH and FAD obtained from Ref. 29 are presented as EEMs (excitation-emission matrix) in Figs. 1(a) and 1(b). Keratin fluorescence that originates from the periphery of the cells in the superficial and the intermediate layers of the cervical epithelium was observed in a previous study.[13] However, the fluorescence spectra of keratin in tissue have not been previously characterized. Under a differ-

ent study protocol approved by the Institutional Review Boards at UT M.D. Anderson Cancer Center and the University of Texas at Austin, we obtained a fresh biopsy specimen that consisted of only the superficial and the intermediate layers of the cervical epithelium from a patient at the UT M.D. Anderson Cancer Center. Confocal fluorescence microscopy was used to verify that the sample demonstrated the peripheral epithelial cell fluorescence that is characteristic of keratin. The specimen was then placed in a quartz cuvette filled with phosphate-buffered saline (PBS) and its fluorescence EEM, was acquired using a spectrofluorometer (SPEX Fluorolog II, HORIBA Jobin Yvon, Edison, New Jersey) [Fig. 1(c)].

Collagen crosslinks are the major source of fluorescence in the stroma. However, spectral differences are observed among stromal fluorescence measurements from different fresh cervical biopsy specimens, suggesting that multiple fluorophores might contribute to stromal fluorescence. In support of this hypothesis, Sokolov et al. showed that the fluorescence EEMs from three stromal biopsies could be described as the sum of distinct fluorescence profiles centered at different excitation-emission wavelengths.[30] We obtained three different biopsy specimens of the cervical stroma from patients being seen at the UT M.D Anderson Cancer Center and measured their fluorescence EEMs in a PBS-filled quartz cuvette using a spectrofluorometer. Using the Sokolov et al. approach, we determined that the fluorescence EEMs of all three specimens could be described as a linear combination of three EEMs with fluorescence profiles centered at different excitation-emission wavelengths, which were very similar to those re-

ported by Sokolov et al. In model-based parameter estimation, we estimate the stromal fluorescence as a linear combination of these three fluorophores, whose EEMs are shown in Figs. 1(d)–1(f). Based on the fluorescence characteristics, two of the three fluorophores are identified as different types of collagen crosslinks. The fluorescence peak of the first component [Fig. 1(d)], located at 340-nm excitation and 400-nm emission, closely resembles that of enzymatically activated collagen crosslinks, HP (hydroxylysyl pyridinoline) and LP (lysyl pyridinoline), which excite at 325 nm and emit fluorescence at 400 nm [Fig. 2(a)] (Ref. 31). Another type of collagen crosslink is activated by glycosylation. Monnier et al. separated these nonenzymatically formed crosslinks from dura collagen using pepsin and characterized their fluorescence spectra.[32] The fluorescence peak of this cross link is located at 370-nm excitation and 440-nm emission [Fig. 2(b)], similar to that observed in collagen component 2 [Fig. 1(e)]. The source of fluorescence for collagen component 3 is not yet understood.

The excitation light and the fluorescent light are affected by scattering and absorption events in the epithelium and the stroma. Within the model, changes in scattering and absorption are accounted for by adjusting the level of epithelial scattering and stromal hemoglobin absorption. The spectral characteristics of epithelial scattering, shown in Fig. 3(a), are derived from the scattering coefficient calculated from cervical epithelium in Ref. 20 (22 cm^{-1} at 810 nm) and extrapolating the values at different wavelengths by using the proportionality $\mu_s(\lambda) \propto 1/\lambda^x$ identified in Ref. 33, where x was found to be -1.0 ± 0.7 and -0.95 ± 0.7 for a nontumorigenic and tumorigenic cell line, respectively. In the wavelength range between 400 and 600 nm, the spectral characteristics of $1/\lambda^x$ vary at most by 10% as x varies from 0.9 to 1.1. Thus, the value of x was set to 1.1 to extrapolate the epithelial scattering coefficient. Hemoglobin absorption $\mu_{a,\text{total Hb}}$ in the stroma is determined by the relative concentration of oxy- and deoxyhemoglobin as well as the total hemoglobin concentration. The spectral characteristics of oxy- and deoxyhemoglobin are shown in Fig. 3(b). Since variations in stromal scattering have little effect on the total detected fluorescence,[26] its value is set constant to the values reported in Ref. 34. Thickness of the cervical epithelium ranges between 200 and 500 μm (Ref. 35), and in model-based parameter estimation, we used an average value of 300 μm.

In fitting model to the data, nine parameters are varied, representing changes in the concentrations of NADH, FAD, keratin, each of the three components of collagen, oxy- and deoxyhemoglobin, and epithelial scattering. In the fitting process, the sum of the squared error between the measured EEM and the EEM generated by the forward model is minimized by iteratively adjusting the nine parameters. In the fitting process, the spectral line shapes associated with these nine parameters remain constant, but their magnitudes are adjusted with scaling variables. For example, the epithelial scattering coefficient $\mu_s(\lambda; i)$ at wavelength λ and at iteration i is defined by $\mu_s(\lambda; i) = C_{\text{epi}}^{\text{sct}}(i) \mu_s^*(\lambda)$, where $C_{\text{epi}}^{\text{sct}}(i)$ is the scaling variable at the iteration and $\mu_s^*(\lambda)$ is the baseline epithelial scattering [Fig. 3(a)] at wavelength λ. At each iteration i, nine scaling variables are adjusted by the trust-region-based nonlinear optimization method[36] to minimize the squared error between

the measured fluorescence spectrum $F^{(\lambda_x, \lambda_m)}$ and the analytical, forward model $M(\ )$ by adjusting the nine scaling variables:

$$\sum_{\lambda_x, \lambda_m}^{i} \{F^{(\lambda_x, \lambda_m)} - M[C_{\text{NADH}}^{\text{fl}}(i), C_{\text{FAD}}^{\text{fl}}(i), C_{\text{SE}}^{\text{fl}}(i), C_{\text{Col1}}^{\text{fl}}(i),$$
$$C_{\text{Col2}}^{\text{fl}}(i), C_{\text{Col3}}^{\text{fl}}(i), C_{\text{epi}}^{\text{sct}}(i), C_{\text{Hb}}^{\text{abs}}(i), C_{\text{O}_2}^{\text{sat}}(i)]\}^2,$$

where λ_x and λ_m are excitation and emission wavelengths, respectively. Table 1 summarizes the nine variable parameters in the object function.

To validate that the fitting algorithm yielded good estimates of chromophore concentrations, we used Monte Carlo techniques to simulate a set of EEMs with known optical properties for the epithelium and stroma. The model was then applied to these data and parameters extracted were compared to the true values. Spectra with optical properties representative of normal and dysplastic cervical tissue were included in this test set. The details of the Monte Carlo simulations as well as the optical parameters used in the simulation can be found in Ref. 26. Briefly, the Monte Carlo simulations are based on two-layered tissue with a finite-thickness epithelium and a semiinfinite stroma. The simulations were performed using optical parameters of normal and abnormal tissue at excitation wavelength 350 nm and 12 emission wavelengths between 400 and 640 nm, sampled at 20-nm increments. One million photons were simulated to generate fluorescence spectra for normal tissue and for abnormal tissue at each emission wavelength. The value of each optical parameter estimated by the mathematical model was compared with those that were used in the Monte Carlo simulations.

2.4 Statistical Analysis

To investigate the effects of age and menopausal status on the optical parameters of cervical tissue estimated from the set of clinical data, we divided the patients into three different age groups for subsequent analysis: premenopausal patients below the age of 40 yr old (preM40−), premenopausal patients greater than or equal to the age of 40 yr old (preM40+), and postmenopausal patients (postM). Previous work has shown that fluorescence intensity varies with age and with menopausal status.[15] To evaluate the diagnostic potential of the estimated optical parameters, patients in each age group were further subdivided into three classes based on the histopathologic diagnosis: SN, LGSIL, and HGSIL. Statistical difference between two age groups in a diagnostic class or two diagnostic classes in an age group was tested using the standard Wilcoxon rank-sum test. All statistical analysis was performed using Matlab software (Mathworks, Natick, Massachusetts). Statistical significance was accepted at $p < 0.05$.

3 Results

Figure 4 shows the result of applying the mathematical model to the target fluorescence spectra generated by Monte Carlo simulations using a set of optical parameters representative of normal and precancerous cervical tissue. The spectra that resulted from the mathematical model show good agreement with the target spectra for both the normal case [Fig. 4(a)] and the precancerous case [Fig. 4(b)]. Figures 4(c) and 4(d) com-
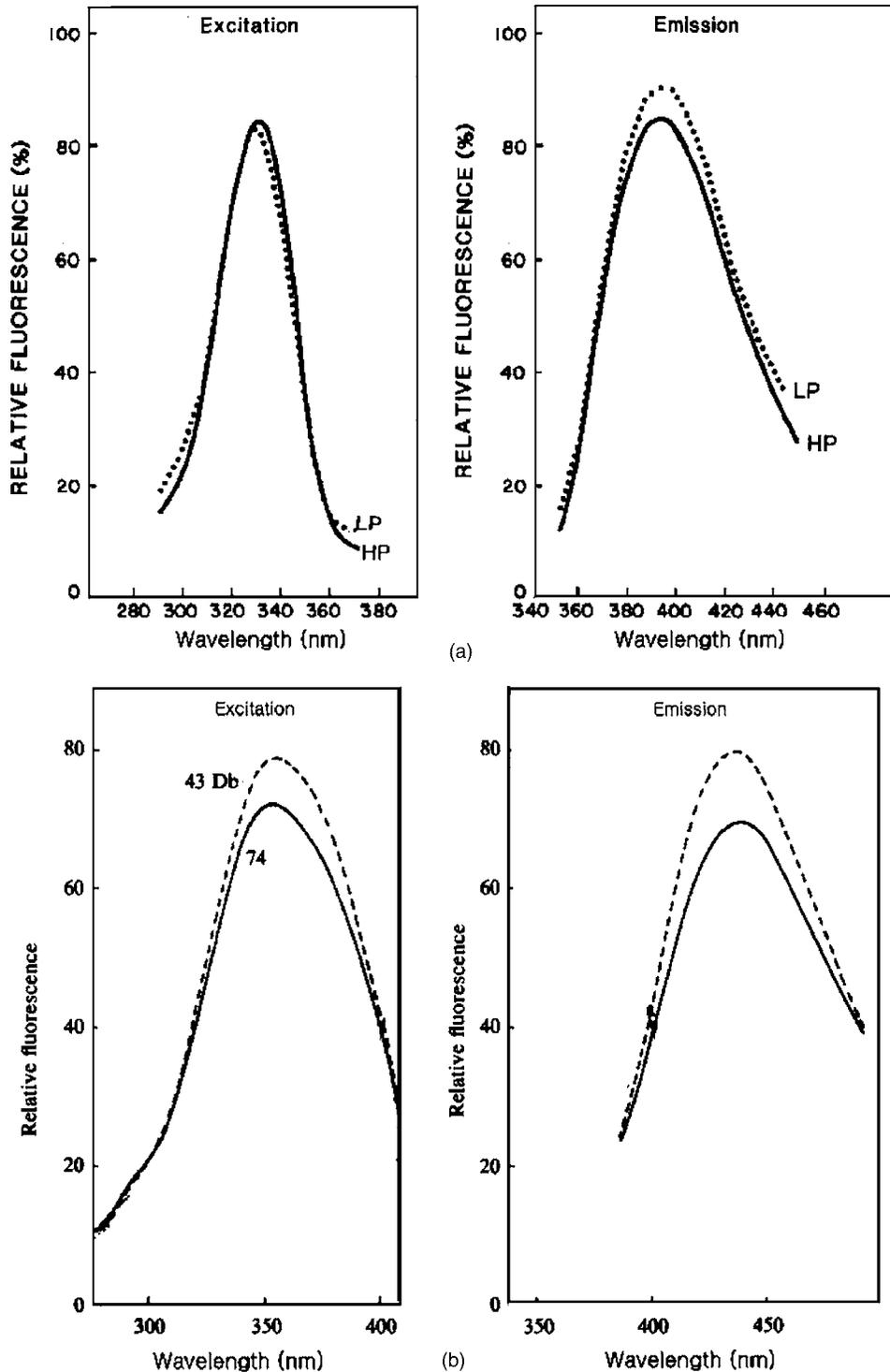
Fig. 2 Fluorescence spectra of two different types of collagen crosslinks: (a) the fluorescence excitation and emission spectra of HP (hydroxylysyl pyridinoline) and LP (lysyl pyridinoline) that are formed by the enzyme lysyl oxidase (modified from Ref. 31) and (b) fluorescence excitation spectrum at 440-nm emission and emission spectrum at 370-nm emission of a collagen crosslink that is formed by glycosylation (modified from Ref. 32). Fluorescence spectra in (b) are acquired from dura collagen of a nondiabetic 74-yr-old (solid plot) and a 43-yr-old diabetic patient (dotted plot).

pare the parameters extracted from the mathematical model to the known values used in the Monte Carlo simulations for the normal [Fig. 4(c)] and the precancerous [Fig. 4(d)] cases. In both cases, fluorescence contributions from epithelial fluoro-

phores NADH, FAD, keratin, and stromal collagen crosslinks extracted with the mathematical model are in good agreement with the values used in the Monte Carlo simulations. The mathematical model slightly underestimates the stromal fluo-
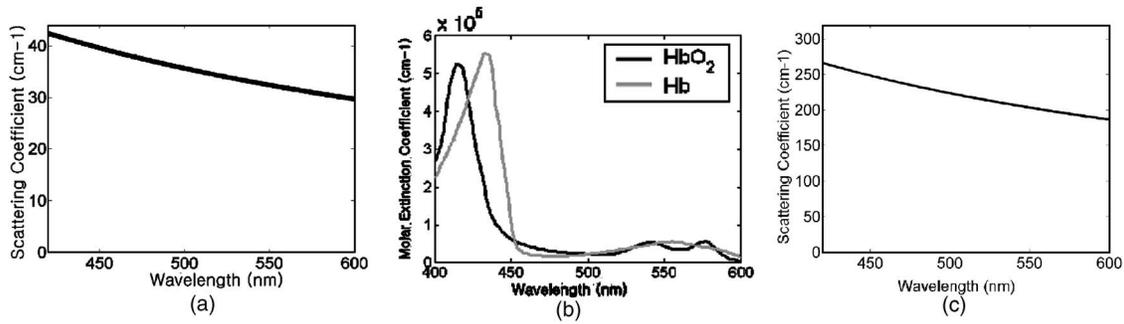
Fig. 3 Spectral characteristics of (a) epithelial scattering derived from Refs. 17 and 20, (b) stromal hemoglobin absorption from S. Prahl, Optical Absorption of Hemoglobin, http://omlc.ogi.edu/spectra/hemoglobin/, Oregon Medical Laser Center, 1999, and (c) stromal scattering from Ref. 34 that are used in the mathematical model.

rescence and the slightly overestimates the epithelial fluorescence when optical parameters of normal tissue are used. This is because the mathematical model overestimates the epithelial scattering in the range where the values are relatively small. When the level of epithelial scattering is higher, as is the case in precancerous tissue, the mathematical model estimates the stromal fluorescence and the epithelial fluorescence more accurately.

Fluorescence spectra were collected from a total of 493 sites in 292 patients using the FastEEM clinical device. Stratification of the measured sites with respect to histopathologic diagnosis and age groups is shown in Table 2. The mathematical model was applied to data from each of these 493 sites to extract the value of the nine optical parameters. Figure 5 presents a comparison of the fitted spectra generated by the math-

ematical model for two typical measurements from a squamous normal site [Fig. 5(a)] and a HGSIL site [Fig. 5(b)] from a single patient. Five fluorescence emission spectra between excitation wavelengths 340 and 380 nm were used in the fitting process. Lower fluorescence intensity is observed in abnormal tissue [Fig. 5(b)] compared to normal tissue [Fig. 5(a)], due to increased epithelial scattering, weaker stromal fluorescence and stronger light absorption due to stromal hemoglobin.[37] The mathematical model was able to accurately describe the fluorescence spectra from both normal tissue and from precancerous tissue; the residual between the measured data and the fitted spectrum (shown in gray) is less than 5% of the fluorescence intensity.

Figure 6 shows the median of each of the nine optical parameters estimated by the mathematical model from the 493 measurements listed in Table 2. The error bars represent one standard deviation. Epithelial scattering from squamous normal samples decreases in preM40+ ($p < 0.005$) and postM ($p < 0.005$) age groups compared to preM40− age group, as shown in Fig. 6(a). However, no significant variation with age is observed among LGSIL samples and HGSIL samples. Within preM40− and postM age groups, epithelial scattering generally increases in LGSIL ($p < 0.005$) and HGSIL ($p < 0.005$) samples compared to squamous normal samples. Similar to epithelial scattering, the level of hemoglobin absorption [Fig. 6(b)] decreases in preM40+ ($p < 0.05$) and postM ($p < 0.005$) age groups compared to preM40− age group among squamous normal samples. Hemoglobin absorption does not change significantly with age among LGSIL and HGSIL samples. In preM40− and postM age groups, hemoglobin absorption increases in LGSIL ($p < 0.05$) and HGSIL ($p < 0.05$) sites compared to squamous normal sites. No significant difference was observed in hemoglobin oxygen saturation among the different age groups or diagnostic cases [Fig. 6(c)].

Figures 6(d)–6(f) show the median fluorescence intensity from the three different epithelial fluorophores in each age group by diagnostic class. NADH fluorescence [Fig. 6(d)] increased in postM age group compared to preM40− age group among squamous normal samples ($p < 0.05$) but did not show significant variation with age among dysplastic samples. NADH fluorescence decreased in LGSIL ($p < 0.005$) and HGSIL ($p < 0.05$) samples compared to squamous normal samples within the postM age group. On the other hand, FAD

Table 1 Table of free parameters varied in the mathematical model.

| Parameter	Description
C_{NADH}^{fl}	Fluorescence efficiency of epithelial fluorophore NADH
C_{FAD}^{fl}	Fluorescence efficiency of epithelial fluorophore FAD
C_{SE}^{fl}	Fluorescence efficiency of superficial epithelial fluorescence
C_{Col1}^{fl}	Fluorescence efficiency of component 1 of stromal fluorescence
C_{Col2}^{fl}	Fluorescence efficiency of component 2 of stromal fluorescence
C_{Col3}^{fl}	Fluorescence efficiency of component 3 of stromal fluorescence
C_{epi}^{sct}	Epithelial scattering
C_{Hb}^{abs}	Stromal hemoglobin absorption
$C_{O_2}^{sat}$	Oxygen saturation of stromal hemoglobin
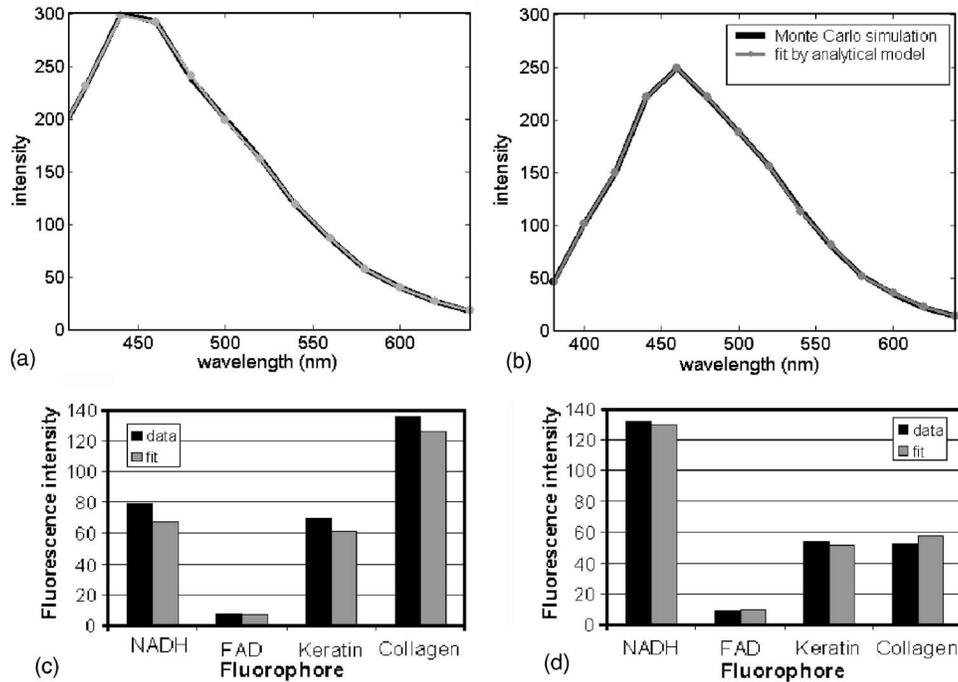
Fig. 4 Results of applying the mathematical model to fluorescence spectra representative of normal tissue (left column) and precancerous tissue (right column) generated using Monte Carlo simulations. (a) and (b) Fluorescence spectra generated by the Monte Carlo simulations shown in thick black lines, while the results of the fit represented by the thin gray lines with circular markers, and (c) and (d) contribution of each of the individual six fluorophores used as input to the Monte Carlo model (black bars) compared to that extracted from the mathematical model (gray bars).

fluorescence increased in LGSIL ($p < 0.005$) and HGSIL ($p < 0.005$) samples compared to squamous normal samples in the preM40− age group, as seen in Fig. 6(e). FAD fluorescence did not very significantly among different age groups. Keratin fluorescence decreased substantially in LGSIL ($p < 0.005$) and HGSIL ($p < 0.005$) samples compared to squamous normal samples in preM40− age group [Fig. 6(f)]. Keratin fluorescence also decreased in LGSIL samples ($p < 0.05$) compared to squamous normal samples in the postM age group.

Median fluorescence intensity from the three stromal fluorophores is shown in Fig. 6(g)–6(i). The fluorescence contribution of all three stromal fluorophores in the squamous normal samples increased in preM40+ ($p < 0.05$) and postM ($p < 0.005$) age groups compared to preM40− age group. Stromal fluorescence from dysplastic samples did not show

strong correlation with age. Dysplastic samples showed decreased stromal fluorescence from collagen component 1 compared to squamous normal samples in all three age groups ($p < 0.005$). Dysplastic samples in the postM age group also showed a decrease in stromal fluorescence from collagen component 2 in dysplastic tissue ($p < 0.05$).

4 Discussion

To estimate each optical parameter accurately, it is important to include all the major endogenous fluorophores in the epithelium and the stroma. We find that there are three fluorophores in the epithelium that exhibit a significant level of fluorescence. The importance of the mitochondrial fluorophores, NADH and FAD, is well known. However, we report a third epithelial fluorophore whose fluorescence originates from the periphery of the epithelial cells that was not well understood. Based on the resemblance of the fluorescence patterns of fresh tissue sections[13] with the immunohistochemical staining patterns of keratin in the epithelium as well as the similarity of the fluorescence characteristics with those of the human fingernail whose major component is keratin (data not shown), this fluorophore is tentatively identified as keratin. Fluorescence from the keratin layer in the epithelium was observed in a number of previous studies. Skala et al.[38] obtained fluorescence images of the keratin layer in normal and malignant hamster cheek pouches using multiphoton laser scanning microscopy at 780-nm excitation. Wu et al.[39] used depth-resolved fluorescence spectroscopy to identify the fluorescence spectrum of keratin at 349-nm excitation from tissue samples of the rabbit esophagus and oral cavity. Although the

Table 2 Number of clinical measurement in three diagnostic categories by age of patients.

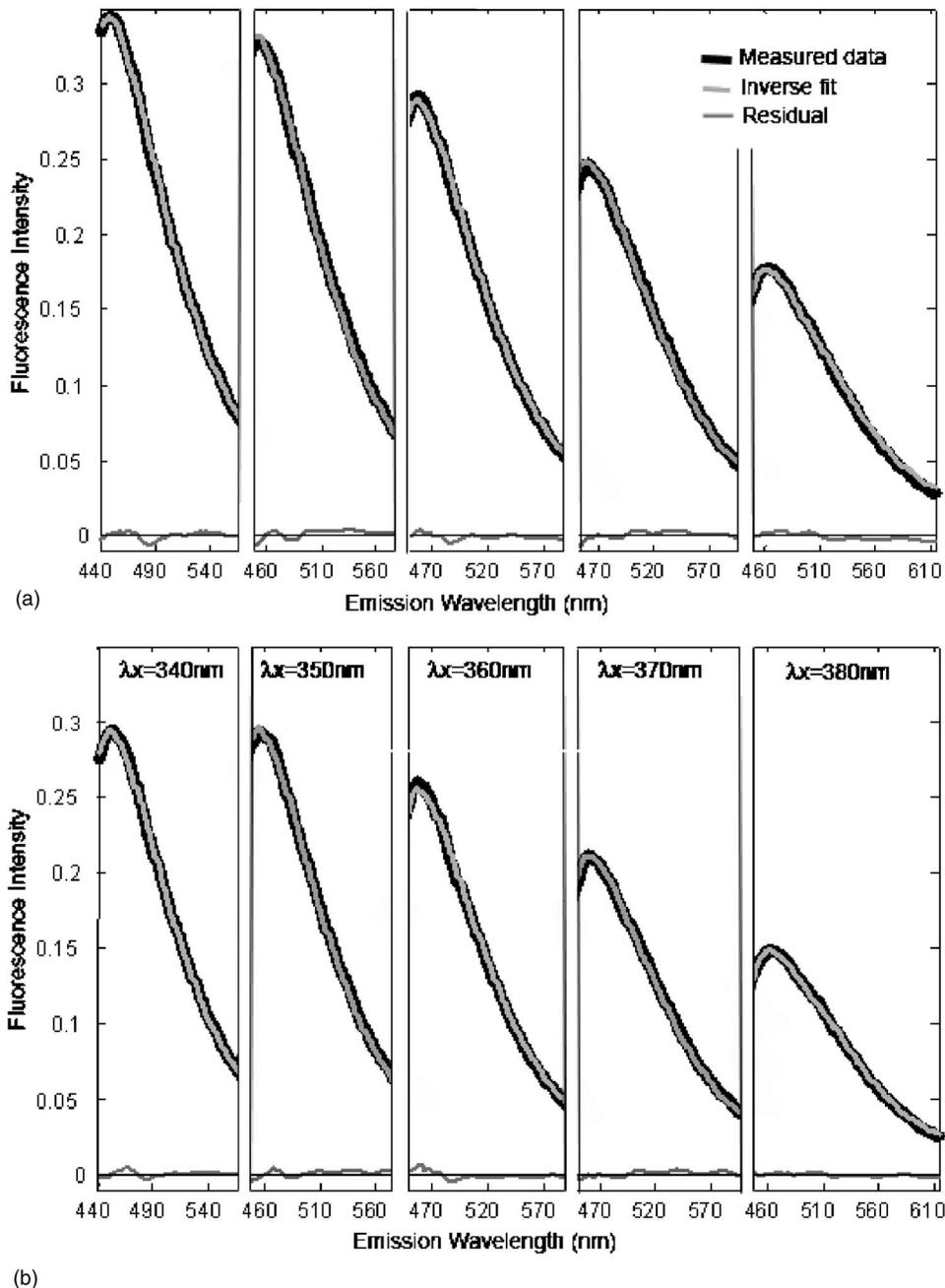|	SN	LGSIL	HGSIL	Total
Premenopausal, <40 y	205	64	121	390
Premenopausal, >40 y	29	9	14	52
Postmenopausal	41	6	4	51
Total	275	79	139	493

Fig. 5 Result of applying the mathematical model to a clinical measurement from (a) a squamous normal site and (b) an HGSIL site. Each plot is a concatenation of 5 emission spectra that were measured at 340-, 350-, 360-, 370-, and 380-nm excitation. In each figure, the thick black line is the fluorescence spectrum from the clinical measurement, and the light gray lines represent the fit generated by the mathematical model. Thin dark gray lines at the bottom of each plot indicate the residual difference between the clinical measurement and the result of the mathematical model.

fluorescence characteristics of keratin as a chemical compound were established previously, this is the first time the fluorescence spectra of endogenous keratin has been measured from fresh cervical epithelial tissue at a wide range of excitation wavelengths.

Fluorescence from the cervical stroma originates from collagen crosslinks, as has been reported by a number of groups. However, the spectral characteristics of stromal fluorescence from cervical biopsies vary significantly between different specimens, suggesting that more than one fluorophore might

be present. We found that data from a large group of patients could not be accurately fit with our mathematical model unless contributions from multiple stromal fluorophores were included. Using curve-fitting techniques, we confirmed the results in Ref. 30 that three different fluorophores are present in the cervical stroma, and we can accurately describe data from a large group of patients when all of these fluorophores are included. Based on previously published fluorescence spectra, we identified two of these three components to be different types of collagen crosslinks: enzymatically activated
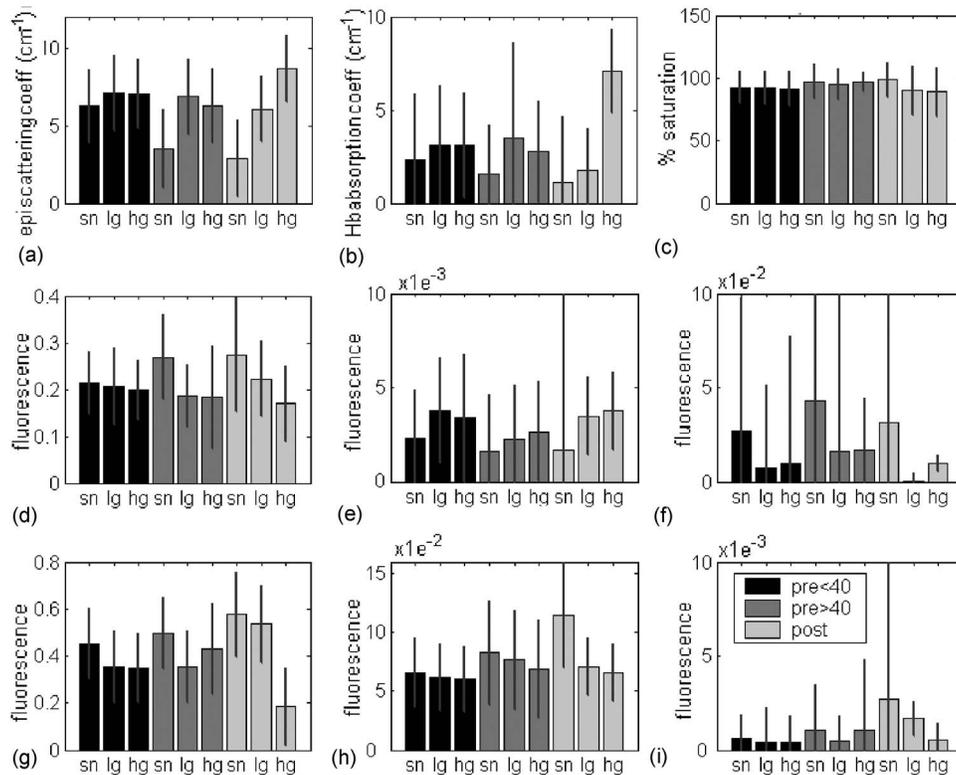
Fig. 6 Median values of the optical parameters extracted from a set of clinical measurements listed in Table 2: (a) epithelial scattering, (b) stromal hemoglobin absorption, (c) oxygen saturation of stromal hemoglobin, (d) fluorescence from NADH, (e) fluorescence from FAD, (f) fluorescence from keratin, (g) fluorescence from collagen component 1 (enzymatically activated collagen crosslinks), (h) fluorescence from collagen component 2 (glycosylated collagen crosslinks), and (i) fluorescence efficiency of collagen component 3. In each figure, the data are classified by three different age groups (black bars for premenopausal patients whose age is below 40 yr old, dark gray bars for premenopausal patients whose age is above 40 yr old, and light gray bars for postmenopausal patients) as well as by diagnostic class (sn for squamous normals, lg for LGSILs, and hg for HGSILs). In each figure, the bar graphs denote the median of the parameters extracted from the corresponding age group and diagnostic class. The error bars show one standard deviation.

crosslinks and glycosylation-activated crosslinks. The density of the enzymatically activated crosslinks increases with collagen fiber maturation and with ageing,[31] and this agrees well with the observed increase in the fluorescence of the first stromal component that we observed with patient age [Fig. 6(f)]. The glycosylation-activated crosslinks are directly related with ageing,[32] and again we observe an age-related increase in the contribution of the second stromal component [Fig. 6(g)].

Using the fluorescence characteristics of the major endogenous fluorophores identified in the epithelium and the stroma, we developed an mathematical model to estimate the relative concentration of these fluorophores as well as the epithelial scattering and hemoglobin absorption from *in vivo* fluorescence measurements. Unlike most of parameter estimation methods developed previously, the model spatially localizes the different fluorophores as well as the scattering and absorption properties to the epithelial and stromal layers. By incorporating the layered structure of epithelial tissue into the model, a more accurate estimation of the optical parameters in each layer can be achieved. In addition, this is the first mathematical model to estimate the keratin fluorescence from the epithelium and to separate the stromal collagen fluorescence into three different fluorophores. Not only does the exhaustive description of fluorophores yield a better estimation of each optical parameter, but it can also lead to the identification of

additional diagnostic markers such as keratin, whose immunohistochemical staining patterns have been correlated with dysplastic progression.[40]

The accuracy of parameter estimation by the mathematical model was validated by applying the model to fluorescence spectra generated by Monte Carlo simulations. Then the mathematical model was applied to a set of *in vivo* fluorescence measurements from cervical tissue. The diagnostic potential of each of the estimated optical parameters, as well as the influence of age and menopausal status on these parameters, were investigated. In the epithelium, FAD fluorescence increases and keratin fluorescence decreases with dysplasia. Since FAD is a cofactor related with cellular metabolic activity, we attribute the increase in FAD fluorescence to increased metabolic activity in abnormal tissue. Increased epithelial fluorescence with dysplastic progression was also observed in previous studies using fresh tissue sections.[13,41] Correlation between keratin fluorescence and dysplastic progression was demonstrated previously using multiphoton laser scanning microscopy, where a decrease in keratin fluorescence following precancerous developments in the hamster cheek pouch model was observed.[38] However, the difference in average fluorescence observed in these hamster cheek pouch microscopy images can be attributed to both a decrease in intrinsic keratin fluorescence and changes in light scattering and ab-

sorption properties. In this study, we were able to extract the intrinsic keratin fluorescence in the epithelium separately from light scattering and absorption and thus demonstrate that the intrinsic keratin fluorescence decreases with dysplasia. The decrease in keratin fluorescence is possibly due to the loss of differentiation in dysplastic epithelium. Immunohistochemical staining studies show that the expression of keratin 10 and 13, markers of terminal differentiation in the exocervix, decrease in precancerous lesions and invasive carcinomas.[40] Fluorescence confocal microscopy images of fresh tissue sections show that the normal epithelium is highly differentiated, and approximately the top half of the epithelium exhibits fluorescence in the cell periphery.[13] On the other hand, abnormal epithelial cells are generally less differentiated, and as more of the epithelium is occupied by dysplastic cells, a decrease in cells showing peripheral fluorescence is expected. The cause of the slight decrease in NADH fluorescence with dysplastic progression is still under investigation.

The decrease in stromal fluorescence with dysplastic progression was observed in previous studies[13,41] and is possibly due to the breakdown of the extracellular matrix by preinvasive, dysplastic cells in the epithelium. However, previous fluorescence microscopy images of the stroma do not differentiate between the three types of fluorophores identified as important here. However, by separating the stromal fluorescence as contribution from three different fluorophores, we were able to conclude that two types of collagen crosslinks as well as a third stromal fluorophore are all affected by dysplastic progression. Stromal fluorescence from squamous normal samples increased with age, which was demonstrated in Ref. 15 using fluorescence microscopy images of fresh tissue sections.

Epithelial scattering and stromal hemoglobin absorption also varied with dysplastic progression. The increase in epithelial scattering in abnormal tissue can be attributed to nuclear atypia that has been shown to increase light scattering.[18] Increased stromal hemoglobin absorption in dysplastic tissue is due to angiogenic developments in the stroma, as demonstrated by diffuse reflectance measurements.[21]

Although most of the optical parameters estimated by the mathematical model show significant variations with dysplasia, they are also affected by biographical factors such as age and menopausal status. For example, although fluorescence from two different collagen crosslinks (one formed enzymatically and the other formed through glycosylation) decreased with dysplasia, they also increased with age. This is congruent with the fact that the density of both of these collagen crosslinks increase with ageing. We have also noticed a decrease in epithelial scattering as well as stromal hemoglobin absorption in older age groups. The causes of these changes are not clear, but they could potentially be attributed to decreased estrogen, decreased cell turnover, and metabolic activity with age.

The fact that most of the estimated optical parameters are affected by dysplastic progression and biographical variables indicates that it is important to consider the various sources of interpatient variation to use these parameters as robust diagnostic markers. For example, the diagnostic significance of stromal fluorescence is more evident among patients in similar age groups than across different age groups. Age and menopausal status identified in this paper are such factors that must be taken into consideration when developing diagnostic tools based on various optical parameters.

In the mathematical model, the epithelial thickness was set to a 300-μm since the introduction of epithelial thickness as a variable parameter could compromise the robustness of the fitting algorithm. Variation in the epithelial thickness from 300 μm to either 200 or 500 μm changes the epithelial and stromal fluorescence detected using the fiber optic probe by up to 25 and 15%, respectively.[26] As a result, the mathematical model reported in this paper could underestimate or overestimate the epithelial and stromal fluorescence if the actual epithelial thickness is not close to 300 μm. Cervical epithelium generally thins with age, but correlation between epithelial thickness and cervical tissue pathology is not clear.[35,42] Thus, the relative degree of estimation error due to changes in epithelial thickness will most likely depend on patient age but will be less prominent among different diagnostic classes within an age group. The overall accuracy of the extracted parameters can be enhanced by applying appropriate average epithelial thickness of the different age groups. However, we found that changes in epithelial fluorescence and scattering associated with high-grade dysplasia generally exceed those expected from this range of variation in values of epithelial thickness.

In summary, we developed a mathematical model to estimate various optical parameters including epithelial scattering, stromal hemoglobin absorption, and the relative concentration of epithelial and stromal fluorophores from *in vivo* fluorescence measurements of cervical tissue. We identified a number of epithelial and stromal fluorophores, and including all of these increases the accuracy of estimating each parameter. Application of the mathematical model to a set of clinical fluorescence measurements showed that most of the estimated optical parameters have high diagnostic potential to discriminate dysplastic tissue from squamous normal tissue.

Acknowledgment

References

1. R. Etzioni, N. Urban, S. Ramsey, M. McIntosh, S. Schwartz, B. Reid, J. Radich, G. Anderson, and L. Hartwell, "The case for early detection," *Nat. Rev. Cancer* **3**, 243–252 (2003).
2. K. Sokolov, M. Follen, and R. Richards-Kortum, "Optical spectroscopy for detection of neoplasia," *Curr. Opin. Chem. Biol.* **6**, 651–658 (2002).
3. U. Utzinger and R. R. Richards-Kortum, "Fiber optic probes for biomedical optical spectroscopy," *J. Biomed. Opt.* **8**, 121–147 (2003).
4. S. K. Chang, M. Follen, A. Malpica, U. Utzinger, G. Staerkel, D. Cox, E. N. Atkinson, C. MacAulay, and R. Richards-Kortum, "Optimal excitation wavelengths for discrimination of cervical neoplasia," *IEEE Trans. Biomed. Eng.* **49**, 1102–1111 (2002).
5. W. K. Huh, R. M. Cestero, F. A. Garcia, M. A. Gold, R. S. Guido, K. McIntyre-Seltman, D. M. Harper, L. Burke, S. T. Sum, R. F. Flewelling, and R. D. Alvarez, "Optical detection of high-grade cervical intraepithelial neoplasia in vivo: results of a 604-patient study," *Am. J. Obstet. Gynecol.* **190**, 1249–1257 (2004).
6. I. Georgakoudi, E. E. Sheets, M. G. Muller, V. Backman, C. P. Crum, K. Badizadegan, R. R. Dasari, and M. S. Feld, "Trimodal spectroscopy for the detection and characterization of cervical precancers in vivo," *Am. J. Obstet. Gynecol.* **186**, 374–382 (2002).
7. R. J. Nordstrom, L. Burke, J. M. Niloff, and J. F. Myrtle, "Identification of cervical intraepithelial neoplasia (CIN) using UV-excited fluorescence and diffuse-reflectance tissue spectroscopy," *Lasers*

Surg. Med. **29**, 118–127 (2001).

8. C. Zhu, G. M. Palmer, T. M. Breslin, F. Xu, and N. Ramanujam, "Use of a multiseparation fiber optic probe for the optical diagnosis of breast cancer," *J. Biomed. Opt.* **10**, 024032 (2005).

9. M. G. Muller, I. Geogakoudi, Q. Zhang, J. Wu, and M. S. Feld, "Intrinsic fluorescence spectroscopy in turbid media: disentangling effects of scattering and absorption," *Appl. Opt.* **40**, 4633–4646 (2001).

10. D. L. Heintzelman, U. Utzinger, H. Fuchs, A. Zuluaga, K. Gossage, A. M. Gillenwater, R. Jacob, B. Kemp, and R. R. Richards-Kortum, "Optimal excitation wavelengths for in vivo detection of oral neoplasia using fluorescence spectroscopy," *Photochem. Photobiol.* **72**, 103–113 (2000).

11. G. M. Palmer, P. J. Keely, T. M. Breslin, and N. Ramanujam, "Autofluorescence spectroscopy of normal and malignant human breast cell lines," *Photochem. Photobiol.* **78**, 462–469 (2003).

12. C. Millot, P. Bondza-Kibangou, J. M. Millot, A. Lallemand, and M. Manfait, "Autofluorescence spectroscopy of malpighian epithelial cells, as a new tool for analysis of cervical cancer precursors," *Histol. Histopathol* **18**, 479–485 (2003).

13. I. Pavlova, K. Sokolov, R. Drezek, A. Malpica, M. Follen, and R. Richards-Kortum, "Microanatomical and biochemical origins of normal and precancerous cervical autofluorescence using laser-scanning fluorescence confocal microscopy," *Photochem. Photobiol.* **77**, 550–555 (2003).

14. I. Georgakoudi, B. C. Jacobson, M. G. Muller, E. E. Sheets, K. Badizadegan, D. L. Carr-Locke, C. P. Crum, C. W. Boone, R. R. Dasari, J. Van Dam, and M. S. Feld, "NAD(P)H and collagen as in vivo quantitative fluorescent biomarkers of epithelial precancerous changes," *Cancer Res.* **62**, 682–687 (2002).

15. C. K. Brookner, M. Follen, I. Boiko, J. Galvan, S. Thomsen, A. Malpica, S. Suzuki, R. Lotan, and R. Richards-Kortum, "Autofluorescence patterns in short-term cultures of normal cervical tissue," *Photochem. Photobiol.* **71**, 730–736 (2000).

16. S. K. Chang, M. Y. Dawood, G. Staerkel, U. Utzinger, E. N. Atkinson, R. R. Richards-Kortum, and M. Follen, "Fluorescence spectroscopy for cervical precancer detection: is there variance across the menstrual cycle?" *J. Biomed. Opt.* **7**, 595–602 (2002).

17. J. R. Mourant, M. Canpolat, C. Brocker, O. Esponda-Ramos, T. M. Johnson, A. Matanock, K. Stetter, and J. P. Freyer, "Light scattering from cells: the contribution of the nucleus and the effects of proliferative status," *J. Biomed. Opt.* **5**, 131–137 (2000).

18. R. Drezek, M. Guillaud, T. Collier, I. Boiko, A. Malpica, C. Macaulay, M. Follen, and R. Richards-Kortum, "Light scattering from cervical cells throughout neoplastic progression: influence of nuclear morphology, DNA content, and chromatin texture," *J. Biomed. Opt.* **8**, 7–16 (2003).

19. D. Arifler, M. Guillaud, A. Carraro, A. Malpica, M. Follen, and R. Richards-Kortum, "Light scattering from normal and dysplastic cervical cells at different epithelial depths: finite-difference time-domain modeling with a perfectly matched layer boundary condition," *J. Biomed. Opt.* **8**, 484–494 (2003).

20. T. Collier, D. Arifler, A. Malpica, M. Follen, and R. Richards-Kortum, "Determination of epithelial tissue scattering coefficient using confocal microscopy," *IEEE J. Quantum Electron.* **9**, 307–313 (2003).

21. G. Zonios, L. T. Perelman, V. M. Backman, R. Manoharan, R. Fitzmaurice, J. Van Dam, and M. S. Feld, "Diffuse reflectance spectroscopy of human adenomatous colon polyps in vivo," *Appl. Opt.* **38**, 6628–6637 (1999).

22. J. Wu, M. S. Feld, and R. P. Rava, "Analytical model for extracting intrinsic fluorescence in turbid media," *Appl. Opt.* **32**, 3585–3595 (1993).

23. M. S. Nair, N. Ghosh, N. S. Raju, and A. Pradhan, "Determination of optical parameters of human breast tissue from spatially resolved fluorescence: a diffusion theory model," *Appl. Opt.* **41**, 4024–4035 (2002).

24. J. C. Finlay and T. H. Foster, "Recovery of hemoglobin oxygen saturation and intrinsic fluorescence with a forward-adjoint model," *Appl. Opt.* **44**, 1917–1933 (2005).

25. D. Stasic, T. J. Farrell, and M. S. Patterson, "The use of spatially resolved fluorescence and reflectance to determine interface depth in layered fluorophore distributions," *Phys. Med. Biol.* **48**, 3459–3474 (2003).

26. S. K. Chang, D. Arifler, R. Drezek, M. Follen, and R. Richards-Kortum, "Analytical model to describe fluorescence spectra of normal and preneoplastic epithelial tissue: comparison with Monte Carlo simulations and clinical measurements," *J. Biomed. Opt.* **9**, 511–522 (2004).

27. R. J. Kurman, Ed., *Pathology of the Female Genital Tract*, Springer-Verlag, New York (1987).

28. N. Marin, N. MacKinnon, C. MacAulay, S. K. Chang, E. Atkinson, D. Cox, D. Serashitopol, M. Follen, and R. Richards-Kortum, "Calibration standards for multi-center clinical trials of fluorescence spectroscopy for in vivo diagnosis," *J. Biomed. Opt.* **11**(1), 014010 (2006).

29. R. S. DaCosta, H. Andersson, and B. C. Wilson, "Molecular fluorescence excitation-emission matrices relevant to tissue spectroscopy," *Photochem. Photobiol.* **78**, 384–392 (2003).

30. K. Sokolov, J. Galvan, A. Myakov, A. Lacy, R. Lotan, and R. Richards-Kortum, "Realistic three-dimensional epithelial tissue phantoms for biomedical optics," *J. Biomed. Opt.* **7**, 148–156 (2002).

31. D. R. Eyre, M. A. Paz, and P. M. Gallop, "Cross-linking in collagen and elastin," *Annu. Rev. Biochem.* **53**, 717–748 (1984).

32. V. M. Monnier, R. R. Kohn, and A. Cerami, "Accelerated age-related browning of human collagen in diabetes mellitus," *Proc. Natl. Acad. Sci. U.S.A.* **81**, 583–587 (1984).

33. J. R. Mourant, J. P. Freyer, A. H. Hielscher, A. A. Eick, D. Shen, and T. M. Johnson, "Mechanisms of light scattering from biological cells relevant to noninvasive optical-tissue diagnostics," *Appl. Opt.* **37**, 3586–3593 (1998).

34. I. S. Saidi, "Transcutaneous optical measurement of hyperbilirubinemia in Neonates," Thesis (1992).

35. D. C. Walker, B. H. Brown, A. D. Blackett, J. Tidy, and R. H. Smallwood, "A study of the morphological parameters of cervical squamous epithelium," *Physiol. Meas* **24**, 121–135 (2003).

36. J. J. More and D. C. Sorensen, "Computing a trust region step," *SIAM (Soc. Ind. Appl. Math.) J. Sci. Stat. Comput.* **4**, 553–572 (1983).

37. R. Drezek, K. Sokolov, U. Utzinger, I. Boiko, A. Malpica, M. Follen, and R. Richards-Kortum, "Understanding the contributions of NADH and collagen to cervical tissue fluorescence spectra: modeling, measurements, and implications," *J. Biomed. Opt.* **6**, 385–396 (2001).

38. M. C. Skala, J. M. Squirrell, K. M. Vrotsos, J. C. Eickhoff, A. Gendron-Fitzpatrick, K. W. Eliceiri, and N. Ramanujam, "Multiphoton microscopy of endogenous fluorescence differentiates normal, precancerous, and cancerous squamous epithelial tissues," *Cancer Res.* **65**, 1180–1186 (2005).

39. Y. C. Wu, P. Xi, J. A. Y. Qu, T. H. Cheung, and M. Y. Yu, "Depth-resolved fluorescence spectroscopy reveals layered structure of tissue," *Opt. Express* **12**, 3218–3223 (2004).

40. C. Carrilho, M. Alberto, L. Buane, and L. David, "Keratins 8, 10, 13, and 17 are useful markers in the diagnosis of human cervix carcinomas," *Hum. Pathol.* **35**, 546–551 (2004).

41. R. Drezek, C. Brookner, I. Pavlova, I. Boiko, A. Malpica, R. Lotan, M. Follen, and R. Richards-Kortum, "Autofluorescence microscopy of fresh cervical-tissue sections reveals alterations in tissue biochemistry with dysplasia," *Photochem. Photobiol.* **73**, 636–641 (2001).

42. M. Guillaud, D. Cox, K. Adler-Storthz, A. Malpica, G. Staerkel, J. Matisic, D. Van Niekerk, N. Poulin, M. Follen, and C. MacAulay, "Exploratory analysis of quantitative histopathology of cervical intraepithelial neoplasia: objectivity, reproducibility, malignancy-associated changes, and human papillomavirus," *Cytometry* **60**, 81–89 (2004).